

# Phosphoproteomic profiling of oxycodone-treated spinal cord of rats with cancer-induced bone pain

HOU-SHENG DENG<sup>1</sup>, LONG-SHENG XU<sup>1</sup>, HUA-DONG NI<sup>1</sup>, YUN-GONG WANG<sup>2</sup>,  
HONG-BO LI<sup>1</sup>, QIU-LI HE<sup>1</sup>, MIAO XU<sup>1</sup> and MING YAO<sup>1</sup>

<sup>1</sup>Department of Anesthesiology and Pain Medicine, The First Affiliated Hospital of Jiaxing University, Jiaxing, Zhejiang 314001; <sup>2</sup>Department of Anesthesiology, Zhuzhou Central Hospital, Zhuzhou, Hunan 412000, P.R. China

Received December 23, 2018; Accepted August 30, 2019

DOI: 10.3892/mmr.2019.10702

**Abstract.** Treatment of cancer-induced bone pain (CIBP) is challenging in clinical settings. Oxycodone (OXY) is used to treat CIBP; however, a lack of understanding of the mechanisms underlying CIBP limits the application of OXY. In the present study, all rats were randomly divided into three groups: The sham group, the CIBP group, and the OXY group. Then, a rat model of CIBP was established by inoculation of Walker 256 tumor cells from rat tibia. Phosphoproteomic profiling of the OXY-treated spinal dorsal cords of rats with CIBP was performed, and 1,679 phosphorylated proteins were identified, of which 160 proteins were significantly different between the CIBP and sham groups, and 113 proteins were significantly different between the CIBP and OXY groups. Gene Ontology analysis revealed that these proteins mainly clustered as synaptic-associated cellular components; among these, disks large homolog 3 expression was markedly increased in rats with CIBP and was reversed by OXY treatment. Subsequent domain analysis of the differential proteins revealed several significant synaptic-associated domains. In conclusion, synaptic-associated cellular components may be critical in OXY-induced analgesia in rats with CIBP.

## Introduction

Cancer-induced bone pain (CIBP) is a common symptom of patients with advanced cancer, which seriously affects their quality of life (1,2). Although pain is common in patients with bone cancer, effectively preventing and controlling CIBP remains one of the most difficult tasks for pain management professionals (3-5). In recent years, oxycodone (OXY) has become the first line of treatment for CIBP (6). OXY is a semi-synthetic opioid analgesic derived from the naturally occurring thebaine (7). An improved understanding of the mechanism of action of OXY is required due to the increase in the number of OXY-dependent patients and cases of mortality caused by OXY overuse (8,9).

The phosphorylation of certain molecules in the central and peripheral nerves can cause hyperalgesia in rats with CIBP (10,11). For example, the phosphorylation of calmodulin can activate a variety of signaling pathways to promote inflammatory factors (12,13). OXY, a G protein-coupled receptor agonist, inhibits adenylate cyclase activity, thereby inhibiting cAMP production which affects the phosphorylation of membrane proteins (14). In nerve cells, the phosphorylation of membrane proteins alters the permeability of certain ions, including calcium ions, resulting in increased calcium influx (15). OXY exerts analgesic effects by inhibiting adenylate cyclase activity and regulating the phosphorylation of cellular proteins (14,15). However, the majority of previous studies have focused on the role of a specific molecule (16,17). At present, little is known regarding the alterations in the phosphorylated protein profile in spinal dorsal horn tissue from rats with bone cancer-induced pain. Therefore, the effect of OXY on the phosphorylated protein profile of spinal dorsal horn tissue during the treatment of rats with CIBP requires further investigation. In the present study, tandem mass tag (TMT) phosphorylation proteomics was used to analyze the phosphorylated molecular signal of OXY in rats with CIBP.

As an essential complement to the postgenomic era, proteomics techniques have been used to study the proteome expression levels in various animal pain models (18-20). Quantitative phosphorylation proteomics analysis based on the isobaric tag for relative and absolute quantitation/TMT is one of the most commonly used methods, having numerous advantages over gel technology, and can directly quantify and

---

*Correspondence to:* Professor Ming Yao, Department of Anesthesiology and Pain Medicine, The First Affiliated Hospital of Jiaxing University, 1882 Zhong-Huan-South Road, Jiaxing, Zhejiang 314001, P.R. China  
E-mail: jxyaoming666@163.com

*Abbreviations:* CIBP, cancer-induced bone pain; DLG3, disks large homolog 3; GO, Gene Ontology; LC, liquid chromatography; MAGUK, membrane-associated guanylate kinase; MS, mass spectrometry; NMDA, N-methyl-D-aspartic acid; OXY, oxycodone; PDZ, postsynaptic density-95 (PSD-95)/Disks large zonaoccludens-1; PWT, paw withdrawal threshold; TMT, tandem mass tag

*Key words:* cancer-induced bone pain, oxycodone, phosphoproteomics, tandem mass tag, disks large homolog 3

compare protein levels in samples with greater efficiency and accuracy (21). Information concerning up- or downregulation of phosphorylated proteins or kinases can be obtained using TMT proteomics techniques, which aid predictions of potential signal transduction processes (22). The purpose of the present study was to obtain a phosphorylated protein profile of the spinal cord dorsal horn tissue of rats with CIBP before and after OXY administration using the TMT phosphorylation proteomics method. The present findings may provide novel insight into the mechanism underlying CIBP and the effects of OXY on hyperalgesia.

## Materials and methods

**Animals.** Adult female Sprague-Dawley rats (9 weeks old,  $n=99$ ), weighing 180–220 g, were purchased from ZheJiang Academy of Medical Sciences and were housed in a 12-h dark/light environment at 22–24°C with a relative humidity of 40–60%. Food and water were freely accessible. The rats were acclimated to the environment for 5 days prior to the experiments. They were 33 rats per group in the study for the various assays; 12 rats in each group were used to evaluate the PWT and the X-ray of the tibia in rats with CIBP, 21 rats in each group were used for protein quantitative analysis and WB analysis, and 3 rat tibias were used for HE staining. All animal experiments and protocols were approved by the Jiaying University Institutional Animal Care and Use Committee, and were performed in accordance with the Association for Assessment and Accreditation of Laboratory Animal Care (<http://www.aaalac.org/accreditation/rules.cfm>) and the Institutional Animal Care and Use Committee (<https://blink.ucsd.edu/sponsor/iaacuc/links.html#Guidelines>) guidelines. All rats were sacrificed by intraperitoneal injection of excess pentobarbital (100 mg/kg). Death was verified by a lack of cardiac pulse, and fixed and diluted pupils.

**Tumor cell preparation.** Tumor cells were prepared as described previously (23–26). Walker 256 rat breast tumor cells were donated by Nanjing University. Walker-256 cells were grown in Dulbecco's modified Eagle medium containing 4.5 g/l glucose, 100 mg/l penicillin, 100 mg/l streptomycin, supplemented with 10% fetal bovine serum and 5% carbon dioxide at 37°C. The cells (0.5 ml;  $2 \times 10^7$  cells/ml) were intraperitoneally injected into the female rats. After a week, ~5 ml of ascites was extracted from the rats, then centrifuged at  $2,500 \times g$  for 3 min at 4°C, then washed with PBS and suspended in D-Hank solution (PB180321, Procell Life Science & Technology Co., Ltd.) to reach a final concentration of  $1 \times 10^7$  cells/ml. The same concentration of heat-killed tumor cells (obtained by heating at a high temperature) was used in the sham group.

**CIBP model.** Walker 256 tumor cells were injected into the left iliac marrow cavity of rats to simulate the development of CIBP clinical pathophysiology as previously described (23,24,27). Briefly, 10  $\mu$ l Walker 256 cells ( $1 \times 10^7$  cells/ml) were slowly injected into the medullary cavity of the left tibia of rats in the CIBP group after the rats were anesthetized with sodium pentobarbital (60 mg/kg; intraperitoneally). The same method was used for heat-killed cells in rats in the sham group. Finally,

all rats undergoing inoculation were allowed to recover naturally for 3 days prior to experiments.

**Bone X-ray examination.** X-ray examination of the left tibia bone was performed on the 12th and 21st days following cancer cell inoculation to confirm destruction of the tibial bone caused by tumor inoculation. The rats underwent a flat X-ray examination following anesthesia with sodium pentobarbital (60 mg/kg; intraperitoneal injection). Tumor cell infiltration and bone destruction were assessed in the bone using an E-COM Technology Digital Radiographer system ( $n=3$  rats per group; E-COM Technology, Ltd.).

**Histological analysis of bone.** Rats ( $n=3$  per group) were sacrificed with pentobarbital (100 mg/kg; intraperitoneal injection) on the 12th day after tumor inoculation. The tibial tissue surrounding the inoculation site was collected (1 cm total) and fixed for 24 h in the 4% phosphate-buffered paraformaldehyde at 4°C. The tibia was decalcified in 10% EDTA solution for 24 h at 55°C. Subsequently, the tissue was dehydrated, embedded in paraffin and cut into 8- $\mu$ m sections using a microtome (Reichert-Leica RM2235; Leica Microsystems GmbH). The extent of tumor cell infiltration and bone destruction was verified by staining with hematoxylin and eosin. Briefly, the section was placed in Mayer's hematoxylin dye solution (cat. no. H9627; Sigma-Aldrich; Merck KGaA) for 5–7 min at room temperature, and washed with tap water to blue. All images were captured under a fluorescent microscope using a  $\times 10$  or  $\times 20$  objective lens (Olympus BX51; Olympus Corporation).

**Drug administration.** The administration of saline (0.9%) and OXY hydrochloride injection (OxyNorm; 10 mg/ml; Napp Pharmaceuticals, Ltd.) was randomized ( $n=21$ ). OXY was diluted to 0.5 mg/ml with 0.9% saline and intraperitoneally injected at a dose of 2.5 mg/kg twice daily for 5 consecutive days from the 8th day after the injection of tumor cells to establish the CIBP model, as described previously (7,17,28,29). Saline was used in the control group.

**Mechanical allodynia assessment.** The alterations in the pain threshold of the left hind paw of rats, which were represented by paw withdrawal threshold (PWT) values (in g), were evaluated using an electronic von Frey's anesthesia meter (IITC Life Science Inc.). Prior to each test, the rats were placed in a glass box (25x20x20 cm<sup>3</sup>) and were allowed to move freely for 30 min to adapt to the wire mesh platform. The test was repeated three times with a minimum of 5 min between each stimulus. The test was conducted 1 h before (pretest) and 30 min after the second daily saline or drug administration. The test was also conducted 0, 15, 30, 60, 120 and 240 min after last administration. The mean of three tests was used as the PWT value of the hind paw of each rat. All tests were performed by investigators blinded to the experimental group.

**Protein preparation.** The rats were sacrificed 30 min after the last drug or saline administration on the 12th day, and the lumbar enlargement was quickly removed and stored in liquid nitrogen (23) ( $n=21$ ). The tissue sample was mixed with a suitable amount of SDT lysate (4% SDS, 100 mM Tris-HCl, 1 mM DTT; pH 7.6), transferred to a 2-ml centrifuge tube

pre-packed with a suitable amount of quartz sand and homogenized using an MP homogenizer (24x2; 6.0 M/S; 60 sec; twice). Subsequently, the sample was sonicated (80 W; work 10 sec, intermittent 15 sec, cycle 10 times) and kept in boiling water for 15 min. Following centrifugation at 14,000 x g for 40 min at 4°C, the supernatant was filtered through a 0.22- $\mu$ m filter and the filtrate was collected. Protein quantification was performed using the bicinchoninic acid method. The samples were stored at -80°C, and 54 samples were used for liquid chromatography (LC)/mass spectrometry (MS) proteomics analysis, and nine samples were used for western blot analysis.

**TMT labeling.** Each of the six protein samples was labeled as a sample pool, with three sample pools in each group. A total of nine sample pools were used for TMT labeling. Protein samples (100  $\mu$ g) were labeled according to the manufacturer's protocol (TMT 6plex Mass Tag Labeling Kits and Reagents; cat. no. 90068; Thermo Fisher Scientific, Inc.). Briefly, the sham group was labeled with 126, 127N and 127C, and the CIBP group was labeled with 128N, 128C and 129N. The OXY group was labeled with 129C, 130N and 130C.

**Phosphopeptide enrichment.** The labeled peptide solution was freeze-dried, and 1X 1,5-dihydroxybenzoic acid (DHB) buffer was added (5X DHB buffer comprised 3% DHB, 80% acetonitrile and 0.1% trifluoroacetic acid) and diluted with water at a 1:4 ratio. The TiO<sub>2</sub> beads were added to the solution, agitated for 40 min and the solution was centrifuged at 14,000 x g for 40 min at 37°C to remove the supernatant. The beads were transferred to the stopper tip and washed. The elution buffer (10 mM Tris-Cl; pH 8.5) was added for elution, and phosphopeptides were collected, concentrated as previously described (30) and dissolved in 30  $\mu$ l 0.1% formic acid. A total of 20  $\mu$ l was used for MS analysis.

**LC-MS/MS analysis.** A total of 3 sample pools in each group were separated and injected using the Easy nLC1000 nanoliter flow high-performance liquid chromatography (Thermo Scientific EASY-nLC 1000 system, Thermo Fisher Scientific, Inc.). Buffer solution A was 0.1% formic acid in water, and solution B was 0.1% formic acid in acetonitrile (84% for acetonitrile). Furthermore, 95% of solution A was used to balance the column. The samples were loaded from an autosampler onto a loading column (Thermo Scientific Easy column; 2 cm x100  $\mu$ m, 5  $\mu$ m-C18; Thermo Fisher Scientific, Inc.) and then separated using an analytical column (0.075x250 mm, 3  $\mu$ m-C18) at a flow rate of 250 nl/min. The relevant liquid-phase gradients were as follows: 0-220 min, B liquid linear gradient from 0-55%; 220-228 min, B liquid linear gradient from 55-100%; 228-240 min, B fluid maintained at 100%. Next, the samples were analyzed using a Q-Exactive mass spectrometer (Thermo Fisher Scientific, Inc.) following separation using the following parameters: Analysis time, 240 min; detection method, positive ion; parent ion scanning range, 350-1,800 m/z; the primary mass spectrometry resolution, 70,000, m/z 200; automatic gain control target, 3x10<sup>6</sup>; first-level maximum ion-trap time (IT), 20 msec; scan range, 1; and dynamic exclusion time, 30.0 sec; the nitrogen gas temperature was 300°C, the nebulizer pressure 310.28 kpa and the flow rate, 12 l/min.

**Database searching.** Mass spectral analysis raw data for RAW files using Mascot 2.2 (Matrix Science, Ltd.) and Proteome Discoverer 1.4 software (Thermo Fisher Scientific, Inc.) were used for identification and quantitative analysis. The database used in the present study was uniptot\_Rat\_35897\_20170511.fasta with the following search parameters: Enzyme, trypsin; max missed cleavages, 2; fixed modifications, carbamidomethyl I; variable modifications, oxidation (M) phospho (ST) phospho (Y); peptide mass tolerance,  $\pm$ 20 ppm; fragment mass tolerance, 0.1 Da. The results of the filter parameters were peptide false discovery rate  $\leq$ 0.01, as described previously (31). The Proteome Discoverer 1.4 software was used to perform quantitative analysis based on the reported peak intensity of peptide ions. The peptide quantification result was the ratio of the signal intensity value of the label where the reference sample was located to the signal intensity value of other labels. The protein quantification result was the median of the quantitative results of the identified peptides. The final quantification results were normalized by the median of each label to eliminate the error in the amount of sample introduced by human factors in the experiment. Mass spectral data were searched using the Mascot software and analyzed using Proteome Discoverer 1.4 software for phosphopeptides. The Phospho RS score was >50, and Phospho RS site probabilities >75% indicated that the phosphorylation modification had higher credibility (32). The MS data were deposited to the Proteome X change Consortium (<http://www.proteomexchange.org>) with the dataset identifier PXD011729.

**Bioinformatics analysis.** The distribution of individual Gene Ontology (GO) (33,34) classifications in the target and overall protein sets was compared using a right-tailed Fisher's exact test when performing a GO annotation enrichment analysis on the target protein set by Blast2GO (35). The domain enrichment analysis was performed with a right-tailed Fisher's exact test using the Pfam (<http://pfam.xfam.org/>) database. P<0.05 was considered to indicate a statistically significant difference.

**Western blot analysis.** Total protein extracts were obtained from tissue homogenates using RIPA buffer (Sigma) and were quantified using a Bicinchoninic Acid Assay kit (Bio-Rad Laboratories, Inc.). Equal amounts of protein (50  $\mu$ g) were separated by 10% SDS-PAGE and transferred onto a PVDF membrane (EMD Millipore). The membrane was then blocked with 5% non-fat milk for 1 h at room temperature and incubated with primary antibodies overnight at 4°C. The primary antibodies used were as follows: Mouse anti-GAPDH (mouse monoclonal antibody; 1:1,000 dilution; cat. no. ab8245; Abcam) and rabbit anti-disks large homolog 3 (DLG3; rabbit polyclonal antibody; 1:750 dilution; cat. no. ab3438; Abcam). The membrane was incubated with horseradish peroxidase-conjugated secondary goat anti-rabbit IgG antibody (goat polyclonal antibody; 1:3,000 dilution; cat. no. A0545; Sigma-Aldrich; Merck KGaA) for 1 h at room temperature after three washes in TBS with Tween-20 (0.05%). Finally, the optical density of the target tape was analyzed using ImageLab 3.0 software (Bio-Rad Laboratories, Inc.). GAPDH was used as the internal control.

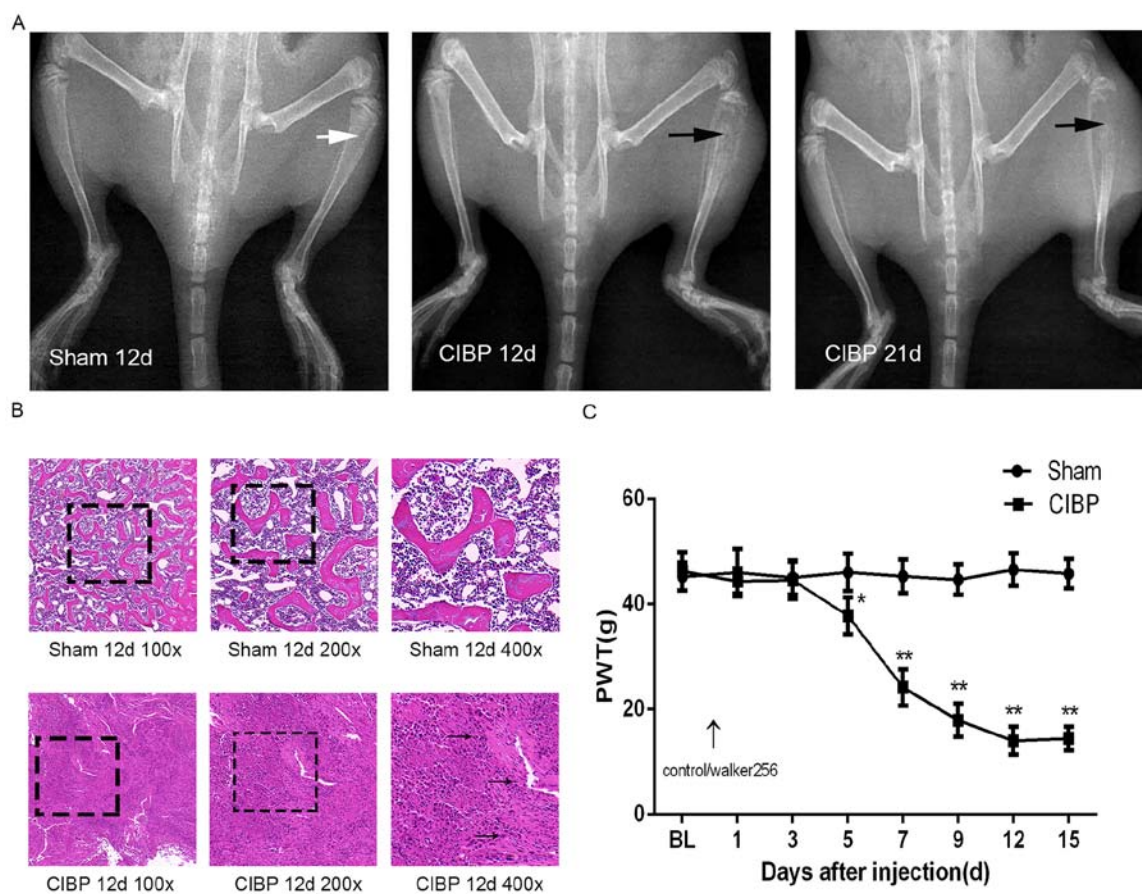


Figure 1. Verification of the CIBP model. (A) Radiographs of tibias following the inoculation of tumor cells. The white arrow points to normal bone structure. The black arrows point to the destruction of the cortical bone that occurred after injection of the tumor cells. (B) Hematoxylin staining of the tibia following tumor inoculation. The malignant tumor cells infiltrated the marrow space on the 8th day after the tumor cell inoculation, as indicated by the black arrows. The magnification (x100, x200 or x400) of the images is indicated in the figure. (C) PWT value of left hind paw following tumor inoculation (arrowed; n=12). The PWT value of the left hind paw in the CIBP group, compared with that in the sham group, began to decrease on the fifth day. One-way ANOVA was used for behavioral analysis. \* $P < 0.05$ , \*\* $P < 0.01$  vs. sham group. BL, baseline; CIBP, cancer-induced bone pain; PWT, paw withdrawal threshold.

**Statistical analysis.** SPSS 21.0 statistical software (IBM Corp.) was used for analysis, and measurement data (n=12) are presented as the mean  $\pm$  SD. One-way ANOVA was used for comparisons among groups followed by the Bonferroni post hoc test; for time course experiments of nociception, repeated-measures ANOVA followed by Bonferroni post hoc test was used.  $P < 0.05$  was considered to indicate a statistically significant difference.

## Results

**Verification of CIBP model.** In the present study, a rat model of CIBP was established by inoculation of Walker-256 breast cancer cells into the medullary cavity of the tibia and the model was subsequently verified by three methods, including X-ray imaging, hematoxylin staining and determination of PWT of the hind paw. No significant changes were observed in the X-ray image of the tibia of the sham group. Cortical bone destruction occurred in the CIBP group rats as indicated by the black arrow on the 12th days after inoculation of tumor cells (Fig. 1A). Hematoxylin staining of the tibia showed that the tumor cells infiltrated into the medullary cavity on 12th days after modeling in the CIBP rats as indicated by the black arrow (Fig. 1B); This phenomenon was not observed in

the sham group. By measuring the PWT of hind paw in rats, it was found that there was no significant difference in the PWT of hind paw in the CIBP group compared with the sham group on baseline (BL;  $P > 0.05$ ). Compared with the control group, the PWT of hind paws was statistically significant ( $P < 0.05$ ) on the fifth day of inoculation of tumor cells in the CIBP group, and the PWT of hind paws continued to decrease, and began to stabilize after the 12th day (Fig. 1C).

**Effects of intraperitoneal injection of OXY on mechanical allodynia in CIBP.** Saline or OXY were intraperitoneally administered in the sham and CIBP groups to examine the effects of OXY on CIBP behavior. The preliminary experiments demonstrated that the onset time of OXY using the systemic administration route was 15 min, with peak efficacy after 30 min and efficacy lasting for 2-4 h (Fig. 2B), which was consistent with the results of previous studies (7,28,36,37). As shown in Fig. 2A, the PWTs in the OXY group were increased significantly 30 min after daily treatment (2.5 mg/kg; intraperitoneally). These results indicated that OXY (2.5 mg/kg; intraperitoneally) reversed the decreased PWTs in the CIBP model.

**Phosphorylated protein atlas in rats with CIBP following OXY treatment.** TMT quantitative phosphoproteomic technology

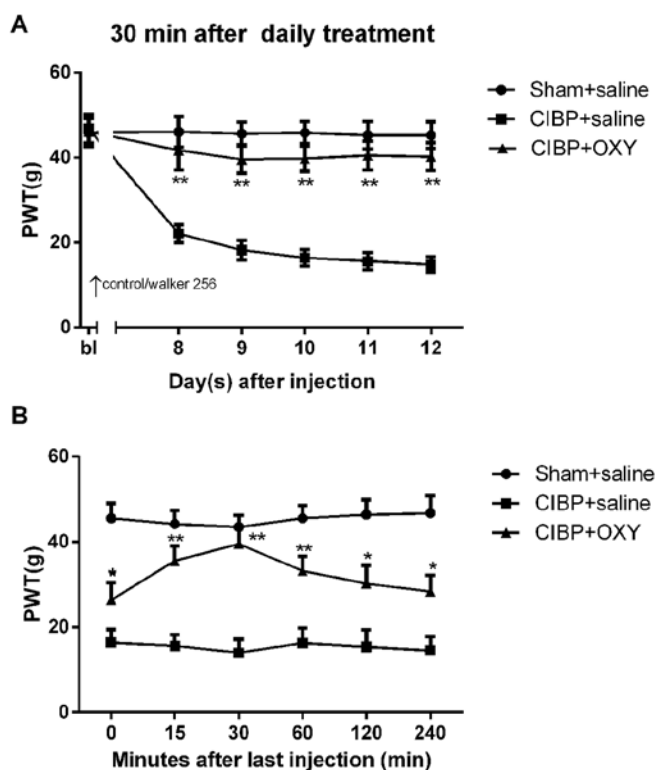


Figure 2. Determination of PWT after OXY treatment. (A) PWTs in the CIBP + OXY group were increased significantly 30 min after daily treatment (2.5 mg/kg; intraperitoneally) compared with those in the CIBP + saline group. (B) Onset time of OXY via the systemic administration route was 15 min, with peak efficacy after 30 min and efficacy lasting for 2-4 h in the CIBP + OXY group compared with in the CIBP + saline group. Behavioral analysis was performed using repeated-measures ANOVA.  $n=12$ . \* $P<0.05$ , \*\* $P<0.01$  vs. CIBP + saline group. BL, baseline; CIBP, cancer-induced bone pain; OXY, oxycodone; PWT, paw withdrawal threshold.

was used in the present study to further investigate the alterations in protein and phosphorylated protein profile of the spinal dorsal horn following the intraperitoneal injection of OXY in rats with CIBP. As a result, a total of 4,863 phosphorylated peptides and 1,679 phosphorylated proteins were identified in all three groups (sham, CIBP and OXY). Additionally, 19,379 phosphosites were identified (Fig. 3A; Table SI). Among all phosphosites, serine accounted for 75.5%, threonine for 20.9% and tyrosine for 3.6% (Fig. 3B). Using a 1.2-fold cut-off for hypophosphorylation and hyperphosphorylation events ( $P<0.05$ ), 217 differentially abundant phosphorylated peptides, including 160 differentially abundant phosphorylated proteins, were identified between the CIBP and sham groups. Compared with the sham group, 114 phosphorylated peptides were upregulated and 103 downregulated in the CIBP group (Fig. 3C; Table SII). A total of 160 differentially abundant phosphorylated peptides, including 113 differentially abundant phosphorylated proteins, were identified between the CIBP and OXY groups. A total of 54 phosphorylated peptides were upregulated and 106 were downregulated in the CIBP group (Fig. 3D; Table SIII). Furthermore, 14 differentially abundant phosphorylated peptides were identified in all three groups (Table I). Notably, the levels of all eight upregulated phosphorylated peptides were decreased and the levels of five downregulated phosphorylated peptides were increased

following OXY treatment in the CIBP group compared with those in the sham group. Only the level of one downregulated phosphorylated peptide remained low following OXY treatment (Table I).

**GO enrichment analysis of cellular components.** GO analysis of the cellular components of differentially abundant phosphorylated proteins between the CIBP and sham groups was performed to ascertain how these differentially abundant phosphorylated proteins contributed to analgesia in rats with CIBP following OXY treatment. The top 10 enriched cellular components in the CBP group are presented in Fig. 4A. The top 10 enriched cellular components between the CIBP and OXY groups are presented in Fig. 4B. Notably, seven GO terms were included in both lists. Of these, six GO terms were closely associated with synaptic function, including GO0044456 ('synapse part'), GO0098794 ('postsynapse'), GO0014069 ('postsynaptic density'), GO0099572 ('postsynaptic specialization'), GO0032279 ('asymmetric synapse') and GO0098984 ('neuron-to-neuron synapse'). A total of 23 differentially abundant phosphorylated proteins were associated with these 6 GO terms between the sham and CIBP groups (Table SIV). Additionally, 22 proteins belonged to these GO terms between the CIBP and OXY groups (Table SV). These were further analyzed as candidate proteins, and included eight common phosphorylated proteins (Tables SIV and SV) represented by a red font. Of note, the levels of five phosphorylated proteins, including phosphorylated microtubule-associated protein 1A, phosphorylated microtubule-associated protein 1B (MAP1B), phosphorylated protein bassoon, phosphorylated erythrocyte membrane protein band 4.1-like 3 and phosphorylated disks large homolog 3 (DLG3), were increased in rats with CIBP compared with in rats in the sham group. However, the levels of these phosphorylated proteins decreased following OXY treatment.

**Domain enrichment analysis of the differential proteins.** Subsequent domain analysis of the differential proteins compared with the sham group suggested several significant synapse-associated domains. Furthermore, these domains were also significantly enriched following OXY treatment of rats with CIBP. The domains included PF04382: 'Spectrin/actin-binding (SAB) domain', PF05902: '4.1 protein C-terminal domain' (CTD) and PF00038: 'intermediate filament protein' (Fig. 5A and B). In addition, the PF00414: 'Neuraxin and MAP1B repeat domains of MAP1B' were significantly enriched in the CIBP group compared with the sham group, whereas this domain was not significantly enriched after OXY administration (Fig. 5A). The PF00625: 'PDZ [postsynaptic density-95 (PSD-95)]/Disks large/zona-occludens-1-associated domain of N-methyl-D-aspartic acid (NMDA) receptors', PF10608: 'polyubiquitination (PEST) N-terminal domain of membrane-associated guanylate kinase (MAGUK)' and PF00625: 'guanylate kinase domains' of the bone cancer pain group were not significantly enriched, whereas these domains were significantly enriched after OXY treatment compared with those in the sham group (Fig. 5B).

**Analysis of non-phosphorylated protein levels.** Combined GO and domain analyses revealed that synapse-associated protein

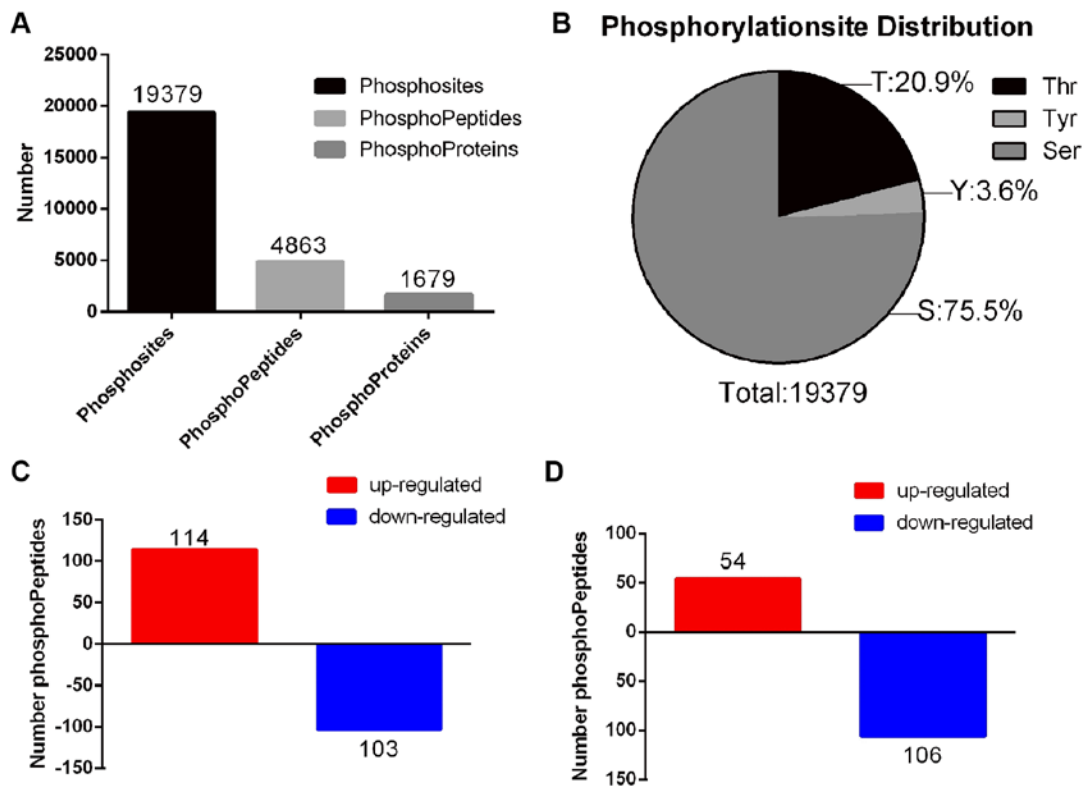


Figure 3. Phosphoproteomic analysis. (A) A total of 1,679 phosphoproteins, 4,863 phosphopeptides and 19,379 phosphosites were identified. (B) Phosphorylation site distribution. (C) Differentially abundant phosphopeptides between the sham and CIBP groups. (D) Differentially abundant phosphopeptides between the CIBP and OXY groups. CIBP, cancer-induced bone pain; OXY, oxycodone.

components exhibited differential enrichment in spinal dorsal horn tissues of rats with CIBP following OXY treatment, and phosphorylated DLG3 may be a key molecule in OXY treatment of CIBP. Subsequently, the levels of non-phosphorylated DLG3 in the spinal dorsal horn tissue were further analyzed using western blot analysis. As shown in Fig. 6, compared with the sham group, the DLG3 levels in the spinal dorsal horn tissues of rats with CIBP were increased, and OXY reduced this effect. It has not been possible to analyze the alterations in phosphorylation levels using western blot analysis due to a lack of phosphorylation site-specific antibodies.

## Discussion

The CIBP rat model induced using Walker 256 mammary tumor cells may simulate the pathogenesis of patients with CIBP, and has been widely used in CIBP research (23-25). Of course, a number of studies have also used a variety of other animal models to study bone cancer pain (38,39). Schwei *et al.* (38) established a mouse femur bone cancer (FBC) pain model by injecting osteolytic mouse sarcoma NCTC2472 cells into the femoral bone marrow cavity. Similar to the FBC model, the injection of NCTC2472 cells into the mouse calcaneus can establish a calcaneus bone cancer pain model (39). However, three types of cancer often cause bone metastases; breast, prostate and lung cancer (2). Therefore, breast cancer cells were used to establish a CIBP model in the present study. In the present study, three methods were used to validate the CIBP rat model, including radiological examination of the left tibia

bone, hematoxylin staining of the tibia and measurement of the PWT of the left hind paw. OXY is an opioid agonist widely used for treating moderate to severe pain in clinical practice (7). A number of clinical and animal studies have demonstrated that OXY reaches peak efficacy at 30 min after systemic administration, with the effects lasting for 2-4 h (7,36,37). Therefore, in the present study, rats were sacrificed 30 min after administration on the 12th day of CIBP rats, and spinal cord tissue was collected for phosphoproteomic analysis. A total of 1,679 phosphoproteins and 4,863 phosphopeptides were identified, in three groups using the TMT phosphorylation technique, in addition to 19,379 phosphorylation sites. Interestingly, 14 differentially phosphorylated peptides belonging to 13 phosphorylated proteins were identified in the three groups. It was inferred that these proteins, including neurofilament heavy polypeptide, DLG3 and microtubule-associated protein, were associated with the analgesic effects of OXY.

In the present study, all differentially abundant phosphoproteins were subjected to GO enrichment analysis. Notably, six synapse-associated GO entries, including GO0044456: 'synapse part', GO0098794: 'postsynapse', GO0014069: 'postsynaptic density', GO0099572: 'postsynaptic specialization', GO0032279: 'asymmetric synapse' and GO0098984: 'neuron-to-neuron synapse', existed in both rankings. Synapses are the functional link between neurons and a key part of information transmission (40,41). Presynaptic calcium influx is a key step in synaptic transmission (42). The neuronal activity triggered by long-term continuous excitatory peripheral evoked impulses can specifically alter the structure and

Table I. Differentially abundant phosphorylated peptides between the CIBP and sham groups, and between the OXY and CIBP groups.

Sequence	Protein IDs	Protein name	Phosphorylation site probabilities (%)	Fold change CIBP/Sham	P-value	Fold change OXY/CIBP	P-value
sPASVksPGEAksPAEAK	P16884; FILRZ7	Neurofilament heavy polypeptide	S(1): 100.0; S(4): 100.0; S(7): 100.0; S(13): 100.0	0.792127	0.030177	1.301539	0.043963
eEITfIDEIPLPsPtAsPGSPRRRP	D4AAS1	G protein-coupled receptor 162	T(4): 37.8; T(5): 37.8; T(10): 79.9; S(14): 86.1; T(16): 86.1; S(18): 86.1; S(22): 86.1; S(32): 0.0	3.394491	0.014797	0.382391	0.029113
gVTSNTsDsESSsk	Q62936	Disks large homolog 3	T(3): 0.0; S(4): 0.1; T(6): 96.9; S(7): 3.0; S(9): 99.7; S(11): 0.1; S(12): 0.1; S(13): 0.1	1.288081	0.016595	0.665242	0.0195
eSPPQPADDGsEePGsETSDAkST	D4A1Q2	Microtubule-associated protein	S(2): 0.0; S(12): 33.0; S(17): 33.0; T(19): 33.0; S(20): 33.0; S(24): 33.0; T(25): 33.0; T(27): 1.8; T(32): 0.3	1.262656	0.019150	0.592023	0.002063
eSEAEsDEssDEdsDSEETsk	Q6LDZ3	Leukocyte common antigen	S(2): 0.0; S(6): 100.0; S(9): 100.0; S(10): 100.0; S(14): 50.0; S(16): 50.0; T(19): 0.1; S(20): 0.0	1.611936	0.025247	0.665296	0.007388
eQGQADkAsEGEEDPGNR	Q4V8H9	Interferon-induced protein with tetratricopeptide repeats 2	S(9): 100.0	1.705975	0.026870	0.644842	0.002323
eALGGNAADsTEDEDQLQNDkER	A0A0G2JXY3	Uncharacterized protein	S(10): 100.0; T(12): 0.0	1.352634	0.033045	0.795199	0.009367
sQEPISNDQkDsDDDkEk	Q9Z1W6	Protein LYRIC	S(1): 0.0; S(6): 0.0; S(12): 100.0	1.244283	0.038597	0.787261	0.026174
aIEEsEsFsD	D3ZKX1	RCG48807, isoform CRA_a	S(5): 100.0; S(6): 100.0; S(8): 100.0; S(10): 100.0; S(11): 100.0; S(13): 100.0	1.573604	0.049062	0.807985	0.046741
vGSEkGsTGsRDGk	Q80XF7	Gap junction $\gamma$ -2 protein	S(3): 0.0; S(7): 100.0; T(8): 0.0; S(10): 100.0	0.75329	0.004827	1.205399	0.016649
sPVPksPVEEVkPkPEAK	G3V7S2	Neurofilament medium polypeptide	S(1): 0.0; S(6): 100.0	0.811632	0.007093	1.298441	0.040118
sPAEAKsPASVksPGEAK	P16884; FILRZ7	Neurofilament heavy polypeptide	S(1): 100.0; S(7): 100.0; S(10): 2.3; S(13): 97.7	1.411921	0.003365	1.282388	0.025597
fAsFIER	P19527	Neurofilament light polypeptide	S(3): 100.0	0.82836	0.040310	1.254364	0.003244
rFsMEDLNk	O35832	Cyclin-dependent kinase 18	S(3): 100.0	0.66579625	0.048207	0.782255	0.030252

Peptides with P&lt;0.05 and fold change &gt;1.2 are listed. CIBP, cancer-induced bone pain; OXY, oxycodone.

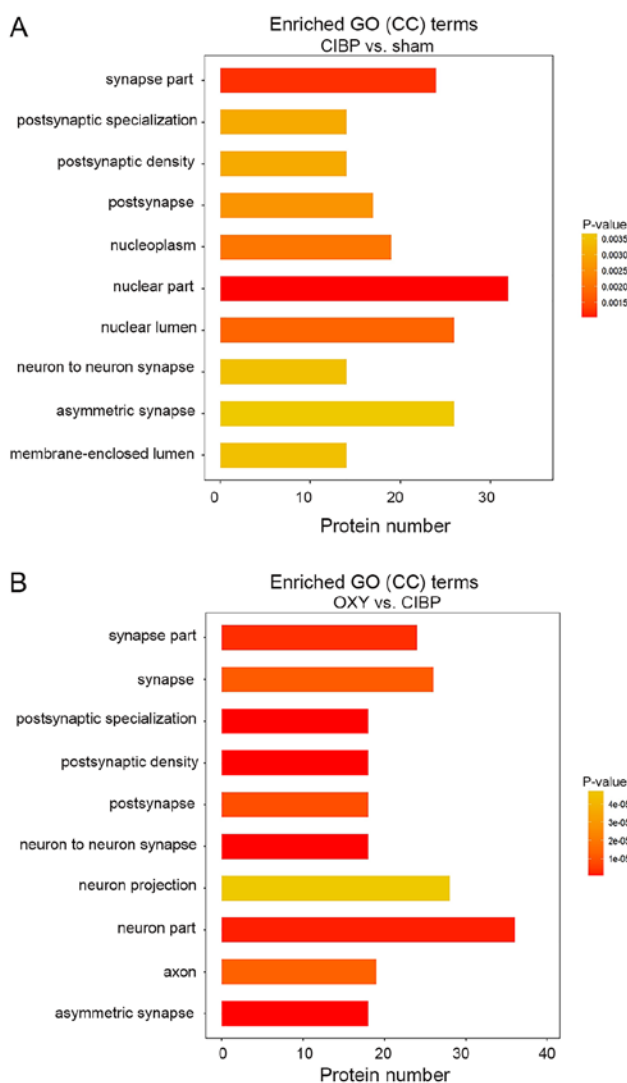


Figure 4. GO enrichment analysis of CC terms. (A) Top 10 CCs between the sham and CIBP groups. (B) Top 10 CCs between the CIBP and OXY groups. Among these, six GO terms were closely associated with synaptic function, including GO0044456 ('synapse part'), GO0098794 ('postsynapse'), GO0014069 ('postsynaptic density'), GO0099572 ('postsynaptic specialization'), GO0032279 ('asymmetric synapse') and GO0098984 ('neuron-to-neuron synapse'). The vertical coordinate is the process name, and the horizontal coordinate is the number of differential proteins enriched. A right-tailed Fisher's exact test was used. The P-value is represented by a color.  $P < 0.05$  was considered to indicate a statistically significant difference. CC, cellular component; CIBP, cancer-induced bone pain; GO, Gene Ontology; OXY, oxycodone.

function of synapses, and this abnormal long-term potentiation of synaptic transmission is crucial in the development of pain (43,44). Phosphorylation modification can regulate synaptic function, and the enhancement of NMDA receptor function in the glutamatergic postsynaptic membrane is central in the formation of central hyperalgesia (44,45). The NMDA receptor-gated channel regulates calcium influx in the postsynaptic membrane (10,42). Intracellular calcium influx leads to the activation of calmodulin, further activating a variety of signaling pathways, which serve important roles in pain transmission (12,13), including the p38-mitogen-activated protein kinase signaling pathway (46). Therefore, synaptic structure and functional adaptation is an important step in the development of central hyperalgesia (43,44,46). MAGUKs located in the postsynaptic density, including DLG3, PSD-95, DLG1 and PSD-93, can anchor NMDA receptors in the postsynaptic membrane (47,48). Their protein interaction with the NMDA receptor enhances the function of glutamatergic excitatory synapses (47,48). The inhibition of postsynaptic

density activity can interfere with NMDA receptor activation and produce an analgesic effect (47,49). In the present study, DLG3 abundance was increased in the spinal dorsal horn tissue in the CIBP group compared with that in the sham group, and OXY administration reversed this effect. This was consistent with the results of previous studies (14,50).

Subsequently, domain enrichment analysis was performed to understand the functional region alterations of these differentially abundant proteins. The results indicated that the domains involved in synapse-associated differential proteins were the PDZ-associated domain of NMDA, polyubiquitination (PEST) N-terminal domain of MAGUK, intermediate filament protein, neuraxin and MAPIB repeat, 4.1 protein-ezrin-radixin-moesin N-terminal domain, 4.1 protein CTD and SAB domain. The differential proteins with PDZ-associated domain of NMDA receptors and a polyubiquitination (PEST) N-terminal domain of MAGUK domains were DLG3 and DLG1 before and after OXY administration in rats with CIBP, respectively. Unexpectedly, no significant difference in this domain was

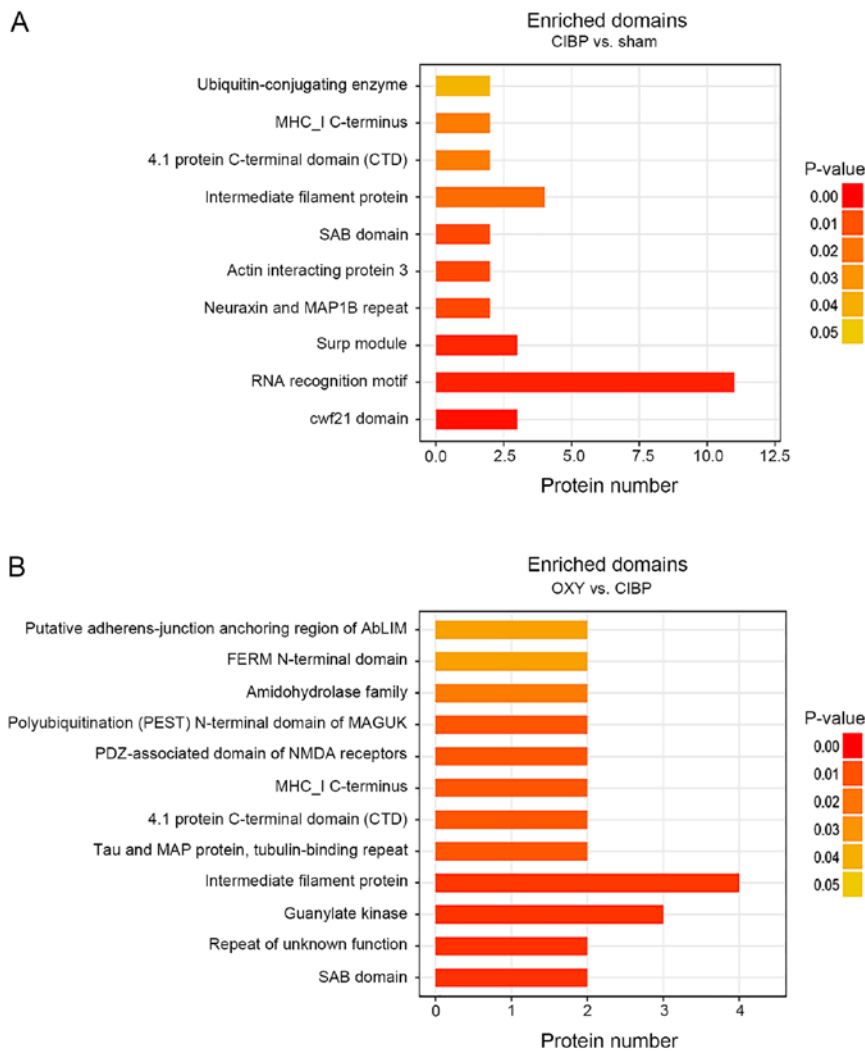


Figure 5. Domain enrichment analysis of differential proteins. (A) Domain enrichment analysis of the differential proteins between the sham and CIBP groups. (B) Domain enrichment analysis of the differential proteins between the CIBP and OXY groups. The vertical coordinate is the name of the domain and the horizontal coordinate is the number of differential proteins enriched. The right-tailed Fisher's exact test was used. Different colors indicate P-values, and  $P < 0.05$  was considered to indicate a statistically significant difference. AblIM, actin-binding LIM protein; CIBP, cancer-induced bone pain; FERM, 4.1 protein ezrin radixin moesin; MAGUK, membrane-associated guanylate kinase; MAP1B, microtubule-associated protein 1B; MHC I, major histocompatibility complex I; NMDA, N-methyl-D-aspartic acid; OXY, oxycodone; PDZ, postsynaptic density-95/disks large zonaoccludens-1; SAB, spectrin and actin binding; Surp module, suppressor-of-white-apricot domain.

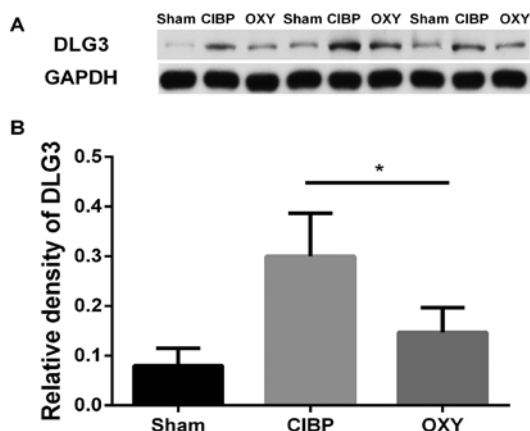


Figure 6. Expression levels of DLG3 in the spinal cord after OXY treatment. (A) Lumbar enlargement was recorded after the last OXY administration on day 12 using western blot analysis ( $n=3$ ). (B) Relative density of DLG3 in the spinal cord after OXY treatment on day 12. One-way ANOVA followed by a Bonferroni post hoc test was used for analysis.  $*P < 0.05$ . CIBP, cancer-induced bone pain; DLG3, disks large homolog 3; OXY, oxycodone.

identified in rats with CIBP compared with the sham group, despite an increase in DLG3 abundance. PDZ-associated domain binds to glutamate NMDA receptor NR2 subunit, promotes NMDA receptor function activation and enhances glutamatergic excitatory synaptic activity (47,48,51). In addition, the N-terminal of DLG3 also possesses a specific NMDA receptor N2B subunit-binding site (47). Phosphorylation of DLG3, which depends on calcineurin activation, promotes the transport of glutamate receptors and their anchoring on the cell membrane (52). It is worth noting that OXY inhibits calcium influx in cells and calmodulin activity (14). In the present study, the decrease in abundance of phosphorylated DLG3 after OXY administration may have been due to the inhibition of calcineurin. This would result in the inhibition of glutamatergic synaptic function (14). Therefore, it was hypothesized that calcineurin was a key kinase for the phosphorylation of synaptic proteins, whereas OXY could cause analgesia by inhibiting phosphorylation kinase activity and regulating synaptic protein phosphorylation. However, the alterations in

abundance of phosphorylated DLG3 were not conclusively due to alterations in the abundance of non-phosphorylated DLG. The focus of future research should be on how OXY regulates the functional regions of synaptic protein phosphorylation.

In conclusion, the present study revealed alterations in the phosphorylated protein profile of spinal cord tissues before and after intraperitoneal injection of OXY in rats with CIBP. By combining phosphorylation proteomics and bioinformatics analysis, the present study provided a novel perspective for further understanding the mechanism underlying bone pain hyperalgesia and the mechanism of action of OXY. The phosphorylation of synapse-associated cellular component proteins may have an important role in the development of hyperalgesia in rats with CIBP.

### Acknowledgements

The authors would like to thank Professor Renshan Ge, the former head of the Endocrinology Lab of the Population Council's Center for Biomedical Research (New York, NY, USA), for assistance with the English language.

### Funding

The present study was supported, in part, by grants from the Natural Science Foundation of Zhejiang Province (grant nos. LY17H090019 and LY16H090016), TCM Research Foundation of Zhejiang Province (grant no. 2016ZA190), Science and Technology Project of Jiaxing City (grant nos. 2017AY33008, 2017AY33020 and 2016AY23033), the National Natural Science Foundation of China (grant nos. 81341035 and 81171057), the Construction Project of Anesthesiology Discipline Special Disease Center in Zhejiang North Region (grant no. 201524) and the Construction Project of Key Laboratory of Nerve and Pain Medicine in Jiaxing City.

### Availability of data and materials

The MS data have been deposited to the Proteome X change Consortium with the dataset identifier PXD011729. The datasets used and/or analyzed during the current study are available from the corresponding author on reasonable request.

### Authors' contributions

MY, LSX and HSD analyzed and interpreted the data. HSD, HDN, YGW, HBL, QLH and MX performed the experiments. HSD was a major contributor in writing the manuscript. All authors read and approved the final manuscript.

### Ethics approval and consent to participate

All animal experiments and protocols were approved by the Jiaxing University Institutional Animal Care and Use Committee (JUMC2018-015) and performed in accordance with AAALAC and IACUC guidelines.

### Patient consent for publication

Not applicable.

### Competing interests

The authors declare that they have no competing interests.

### References

- Harding D, Giles SL, Brown MRD, Ter Haar GR, van den Bosch M, Bartels LW, Kim YS, Deppe M and deSouza NM: Evaluation of quality of life outcomes following palliative treatment of bone metastases with magnetic resonance-guided high intensity focused ultrasound: An international multicentre study. *Clin Oncol (R Coll Radiol)* 30: 233-242, 2018.
- Buga S and Sarria JE: The management of pain in metastatic bone disease. *Cancer Control* 19: 154-166, 2012.
- Mercadante S and Arcuri E: Breakthrough pain in cancer patients: Pathophysiology and treatment. *Cancer Treat Rev* 24: 425-432, 1998.
- Brown M and Farquhar-Smith P: Pain in cancer survivors; filling in the gaps. *Br J Anaesth* 119: 723-736, 2017.
- Frost CØ, Hansen RR and Heegaard AM: Bone pain: Current and future treatments. *Curr Opin Pharmacol* 28: 31-37, 2016.
- Ahmad I, Ahmed MM, Ahsraf MF, Naeem A, Tasleem A, Ahmed M and Farooqi MS: Pain management in metastatic bone disease: A literature review. *Cureus* 10: e3286, 2018.
- Pöyhä R and Kalso EA: Antinociceptive effects and central nervous system depression caused by oxycodone and morphine in rats. *Pharmacol Toxicol* 70: 125-130, 1992.
- Cooper ZD, Bedi G, Ramesh D, Balter R, Comer SD and Haney M: Impact of co-administration of oxycodone and smoked cannabis on analgesia and abuse liability. *Neuropsychopharmacology* 43: 2046-2055, 2018.
- Coe MA, Nuzzo PA, Lofwall MR and Walsh SL: Effects of short-term oxycodone maintenance on experimental pain responses in physically dependent opioid abusers. *J Pain* 18: 825-834, 2017.
- Hanamura K, Washburn H, Sheffler-Collins SL, Xia NL, Henderson N, Tillu DV, Hassler S, Spellman DS, Zhang G, Neubert TA, *et al.*: Extracellular phosphorylation of a receptor tyrosine kinase controls synaptic localization of NMDA receptors and regulates pathological pain. *PLoS Biol* 15: e2002457, 2017.
- Pareek TK, Keller J, Kesavapany S, Agarwal N, Kuner R, Pant HC, Iadarola MJ, Brady RO and Kulkarni AB: Cyclin-dependent kinase 5 modulates nociceptive signaling through direct phosphorylation of transient receptor potential vanilloid 1. *Proc Natl Acad Sci USA* 104: 660-665, 2007.
- Guo N, Zhang X, Huang M, Li X, Li Y, Zhou X and Bai J: Geranylgeranylacetone blocks the reinstatement of morphine-conditioned place preference. *Neuropharmacology* 143: 63-70, 2018.
- Chen SP, Sun J, Zhou YQ, Cao F, Braun C, Luo F, Ye DW and Tian YK: Sinomenine attenuates cancer-induced bone pain via suppressing microglial JAK2/STAT3 and neuronal CAMKII/CREB cascades in rat models. *Mol Pain* 14: 1744806918793232, 2018.
- Vaughan CW, Ingram SL, Connor MA and Christie MJ: How opioids inhibit GABA-mediated neurotransmission. *Nature* 390: 611-614, 1997.
- Scherer PC, Zaccor NW, Neumann NM, Vasavda C, Barrow R, Ewald AJ, Rao F, Sumner CJ and Snyder SH: TRPV1 is a physiological regulator of  $\mu$ -opioid receptors. *Proc Natl Acad Sci USA* 114: 13561-13566, 2017.
- Gaspari S, Cogliani V, Manouras L, Anderson EM, Mitsi V, Avramou K, Carr FB and Zachariou V: RGS9-2 modulates responses to oxycodone in pain-free and chronic pain states. *Neuropsychopharmacology* 42: 1548-1556, 2017.
- Largent-Milnes TM, Guo W, Wang HY, Burns LH and Vanderah TW: Oxycodone plus ultra-low-dose naltrexone attenuates neuropathic pain and associated  $\mu$ -opioid receptor-Gs coupling. *J Pain* 9: 700-713, 2008.
- Zhang Y, Wang YH, Zhang XH, Ge HY, Arendt-Nielsen L, Shao JM and Yue SW: Proteomic analysis of differential proteins related to the neuropathic pain and neuroprotection in the dorsal root ganglion following its chronic compression in rats. *Exp Brain Res* 189: 199-209, 2008.
- Gao Y, Chen S, Xu Q, Yu K, Wang J, Qiao L, Meng F and Liu J: Proteomic analysis of differential proteins related to anti-nociceptive effect of electroacupuncture in the hypothalamus following neuropathic pain in rats. *Neurochem Res* 38: 1467-1478, 2013.

20. Lind AL, Emami Khoonsari P, Sjödin M, Katila L, Wetterhall M, Gordh T and Kultima K: Spinal cord stimulation alters protein levels in the cerebrospinal fluid of neuropathic pain patients: A proteomic mass spectrometric analysis. *Neuromodulation* 19: 549-562, 2016.
21. Mertins P, Udeshi ND, Clauser KR, Mani DR, Patel J, Ong SE, Jaffe JD and Carr SA: iTRAQ labeling is superior to mTRAQ for quantitative global proteomics and phosphoproteomics. *Mol Cell Proteomics* 11: M111.014423, 2012.
22. McAlister GC, Huttlin EL, Haas W, Ting L, Jedrychowski MP, Rogers JC, Kuhn K, Pike I, Grothe RA, Blethrow JD and Gygi SP: Increasing the multiplexing capacity of TMTs using reporter ion isotopologues with isobaric masses. *Anal Chem* 84: 7469-7478, 2012.
23. Mao-Ying QL, Zhao J, Dong ZQ, Wang J, Yu J, Yan MF, Zhang YQ, Wu GC and Wang YQ: A rat model of bone cancer pain induced by intra-tibia inoculation of Walker 256 mammary gland carcinoma cells. *Biochem Biophys Res Commun* 345: 1292-1298, 2006.
24. An K, Rong H, Ni H, Zhu C, Xu L, Liu Q, Chen Y, Zheng Y, Huang B and Yao M: Spinal PKC activation-Induced neuronal HMGB1 translocation contributes to hyperalgesia in a bone cancer pain model in rats. *Exp Neurol* 303: 80-94, 2018.
25. Wang LX and Wang ZJ: Animal and cellular models of chronic pain. *Adv Drug Deliv Rev* 55: 949-965, 2003.
26. Wang Y, Ni H, Li H, Deng H, Xu LS, Xu S, Zhen Y, Shen H, Pan H and Yao M: Nuclear factor kappa B regulated monocyte chemoattractant protein-1/chemokine CC motif receptor-2 expressing in spinal cord contributes to the maintenance of cancer-induced bone pain in rats. *Mol Pain* 14: 1744806918788681, 2018.
27. Liu M, Yao M, Wang H, Xu L, Zheng Y, Huang B, Ni H, Xu S, Zhou X and Lian Q: P2Y<sub>12</sub> receptor-mediated activation of spinal microglia and p38MAPK pathway contribute to cancer-induced bone pain. *J Pain Res* 10: 417-426, 2017.
28. Kato A, Minami K, Ito H, Tomii T, Matsumoto M, Orita S, Kihara T, Narita M and Suzuki T: Oxycodone-induced analgesic effects in a bone cancer pain model in mice. *Oncology* 74 (Suppl 1): S55-S60, 2008.
29. Nielsen CK, Ross FB, Lotfipour S, Saini KS, Edwards SR and Smith MT: Oxycodone and morphine have distinctly different pharmacological profiles: Radioligand binding and behavioural studies in two rat models of neuropathic pain. *Pain* 132: 289-300, 2007.
30. Larsen MR, Thingholm TE, Jensen ON, Roepstorff P and Jørgensen TJ: Highly selective enrichment of phosphorylated peptides from peptide mixtures using titanium dioxide microcolumns. *Mol Cell Proteomics* 4: 873-886, 2005.
31. Wiśniewski JR, Zougman A, Nagaraj N and Mann M: Universal sample preparation method for proteome analysis. *Nat Methods* 6: 359-362, 2009.
32. Olsen JV, Blagoev B, Gnäd F, Macek B, Kumar C, Mortensen P and Mann M: Global, in vivo, and site-specific phosphorylation dynamics in signaling networks. *Cell* 127: 635-648, 2006.
33. Ashburner M, Ball CA, Blake JA, Botstein D, Butler H, Cherry JM, Davis AP, Dolinski K, Dwight SS, Eppig JT, *et al*: Gene ontology: tool for the unification of biology. *The Gene Ontology Consortium. Nat Genet* 25: 25-29, 2000.
34. The Gene Ontology Consortium: The Gene Ontology Resource: 20 years and still GOing strong. *Nucleic Acids Res* 47 (D1): D330-D338, 2019.
35. Götz S, García-Gómez JM, Terol J, Williams TD, Nagaraj SH, Nueda MJ, Robles M, Talón M, Dopazo J and Conesa A: High-throughput functional annotation and data mining with the Blast2GO suite. *Nucleic Acids Res* 36: 3420-3435, 2008.
36. Peckham EM and Traynor JR: Comparison of the antinociceptive response to morphine and morphine-like compounds in male and female Sprague-Dawley rats. *J Pharmacol Exp Ther* 316: 1195-1201, 2006.
37. Lemberg KK, Kontinen VK, Siiskonen AO, Viljakka KM, Yli-Kauhalaoma JT, Korpi ER and Kalso EA: Antinociception by spinal and systemic oxycodone: Why does the route make a difference? In vitro and in vivo studies in rats. *Anesthesiology* 105: 801-812, 2006.
38. Schwei MJ, Honore P, Rogers SD, Salak-Johnson JL, Finke MP, Ramnaraine ML, Clohisey DR and Mantyh PW: Neurochemical and cellular reorganization of the spinal cord in a murine model of bone cancer pain. *J Neurosci* 19: 10886-10897, 1999.
39. Cain DM, Wacnik PW, Turner M, Wendelschafer-Crabb G, Kennedy WR, Wilcox GL and Simone DA: Functional interactions between tumor and peripheral nerve: Changes in excitability and morphology of primary afferent fibers in a murine model of cancer pain. *J Neurosci* 21: 9367-9376, 2001.
40. Li H, Li Y, Lei Z, Wang K and Guo A: Transformation of odor selectivity from projection neurons to single mushroom body neurons mapped with dual-color calcium imaging. *Proc Natl Acad Sci USA* 110: 12084-12089, 2013.
41. Zheng R, Yi X, Lu W and Chen T: Stability of analytic neural networks with event-triggered synaptic feedbacks. *IEEE Trans Neural Netw Learn Syst* 27: 483-494, 2016.
42. Steinert JR, Kopp-Scheinflug C, Baker C, Challiss RA, Mistry R, Haustein MD, Griffin SJ, Tong H, Graham BP and Forsythe ID: Nitric oxide is a volume transmitter regulating postsynaptic excitability at a glutamatergic synapse. *Neuron* 60: 642-656, 2008.
43. Ko HG, Choi JH, Park DI, Kang SJ, Lim CS, Sim SE, Shim J, Kim JI, Kim S, Choi TH, *et al*: Rapid turnover of cortical NCAM1 regulates synaptic reorganization after peripheral nerve injury. *Cell Rep* 22: 748-759, 2018.
44. Chirila AM, Brown TE, Bishop RA, Bellono NW, Pucci FG and Kauer JA: Long-term potentiation of glycinergic synapses triggered by interleukin 1 $\beta$ . *Proc. Natl Acad Sci USA* 111: 8263-8268, 2014.
45. Huang LE, Guo SH, Thitiseranee L, Yang Y, Zhou YF and Yao YX: N-methyl-D-aspartate receptor subtype 2B antagonist, Ro 25-6981, attenuates neuropathic pain by inhibiting postsynaptic density 95 expression. *Sci Rep* 8: 7848, 2018.
46. Lee JO, Kim N, Lee HJ, Lee YW, Kim JK, Kim HI, Lee SK, Kim SJ, Park SH and Kim HS: Visfatin, a novel adipokine, stimulates glucose uptake through the Ca<sup>2+</sup>-dependent AMPK-p38 MAPK pathway in C2C12 skeletal muscle cells. *J Mol Endocrinol* 54: 251-262, 2015.
47. Cui H, Hayashi A, Sun HS, Belmares MP, Cobey C, Phan T, Schweitzer J, Salter MW, Wang YT, Tasker RA, *et al*: PDZ protein interactions underlying NMDA receptor-mediated excitotoxicity and neuroprotection by PSD-95 inhibitors. *J Neurosci* 27: 9901-9915, 2007.
48. Fan J, Cowan CM, Zhang LY, Hayden MR and Raymond LA: Interaction of postsynaptic density protein-95 with NMDA receptors influences excitotoxicity in the yeast artificial chromosome mouse model of Huntington's disease. *J Neurosci* 29: 10928-10938, 2009.
49. Lee WH, Li LL, Chawla A, Hudmon A, Lai YY, Courtney MJ and Hohmann AG: Disruption of nNOS-NOS1AP protein-protein interactions suppresses neuropathic pain in mice. *Pain* 159: 849-863, 2018.
50. Vickers CA, Stephens B, Bowen J, Arbuthnott GW, Grant SG and Ingham CA: Neurone specific regulation of dendritic spines in vivo by post synaptic density 95 protein (PSD-95). *Brain Res* 1090: 89-98, 2006.
51. Cuthbert PC, Stanford LE, Coba MP, Ainge JA, Fink AE, Opazo P, Delgado JY, Komiyama NH, O'Dell TJ and Grant SG: Synapse-associated protein 102/dlg3 couples the NMDA receptor to specific plasticity pathways and learning strategies. *J Neurosci* 27: 2673-2682, 2007.
52. Wei Z, Wu G and Chen BS: Regulation of SAP102 synaptic targeting by phosphorylation. *Mol Neurobiol* 55: 6215-6226, 2018.